

Radio properties of H_2O maser host galaxies

J.S. Zhang¹, C. Henkel^{2,3}, Q. Guo⁴, and J. Wang¹

¹ Center For Astrophysics, GuangZhou University, GuangZhou, 510006, China

² Max-Planck-Institut für Radioastronomie, Auf dem Hügel 69, D-53121 Bonn, Germany

³ Astronomy Department, King Abdulaziz University, P.O. Box 80203, Jeddah 21589, Saudi Arabia

⁴ Hunan Institute of Humanities, Science and Technology, Loudi, 417000, China

received ; accepted

ABSTRACT

The 6 cm and 20 cm radio continuum properties of all 85 galaxies with reported 22 GHz H_2O maser emission and luminosity distance $D > 0.5$ Mpc are studied. For the total of 55 targets for which both 6 cm and 20 cm measurements exist and for the subsample of 42 sources with masers related to active galactic nuclei (AGN), a spectral index could be determined from an assumed power-law dependence. The mean value of the resulting spectral index is in both cases 0.66 ± 0.07 ($S \propto \nu^{-\alpha}$; S : flux density, ν : frequency). Comparing radio properties of the maser galaxies with a sample of Seyferts without detected H_2O maser, we find that (1) the spectral indices agree within the error limits, and (2) maser host galaxies have higher nuclear radio continuum luminosities, exceeding those of the comparison sample by factors of order 5. Only considering the subsample of galaxies with masers associated with AGN, there seems to be a trend toward rising maser luminosity with nuclear radio luminosity (both at 6 cm and 20 cm). However, when accounting for the Malmquist effect, the correlation weakens to a level, which is barely significant. Overall, the study indicates that nuclear radio luminosity is a suitable indicator to guide future AGN maser searches and to enhance detection rates, which are otherwise quite low (<10%).

Key words. Masers – galaxies: active – galaxies: nuclei – radio lines: galaxies – radio continuum: galaxies

1. Introduction

Since the first detection of an extragalactic H_2O maser towards M33 (Churchwell et al. 1977), 22 GHz ($\lambda = 1.3$ cm) H_2O maser surveys have covered ~ 3000 galaxies, with reported detections from 85 objects (e.g., Zhang et al. 2006; Braatz & Gugliucci 2008; Greenhill et al. 2008; Darling et al. 2008). With respect to their physical origin, these maser sources can be subdivided into two classes: (1) those associated with star-forming regions (hereafter SF-masers), which are similar to the stronger sources in the Galaxy, and (2) those associated with active galactic nuclei (hereafter AGN-masers). The majority of the extragalactic H_2O masers are believed to belong to the latter class, mainly because among the small number of interferometrically studied sources, all of the masers with isotropic luminosities $> 10 L_\odot$ are found to be associated with AGN. With their exceptional luminosities, far surpassing those of any galactic maser, these molecular lighthouses are termed “megamasers”. Among AGN maser sources, a large portion ($\sim 40\%$) has been identified as disk maser candidates (Kondratko et al. 2006; Zhang et al. 2010). Their maser spots are located within the central few pc, forming parts of a molecular accretion disk around the nuclear engine. In addition to “systemic” features, “high velocity” components are also found, representing the approaching and receding edges of the disks, which are viewed approximately edge-on. Systematic studies of such disk masers have become a promising tool for addressing a wide variety of astrophysical problems, using both high resolution VLBI (Very Long Baseline Interferometry)

imaging and spectral line monitoring of maser spots (Braatz et al. 2009).

Observations show that H_2O megamasers are mostly associated with the nuclear regions of Seyfert 2 and LINER (low ionizing nuclear emission regions) galaxies, which are commonly heavily obscured (gas column density $N_{\text{H}} > 10^{23} \text{ cm}^{-2}$) (Braatz et al. 1997; Zhang et al. 2006; Greenhill et al. 2008). AGN are considered to be the ultimate energy source of H_2O megamasers (e.g., Lo 2005), so we may expect some kind of correlation between maser power and the nuclear radio luminosity (for its definition, see Sect. 2.1). On the one hand, the nuclear radio continuum luminosity has been established as a useful isotropic luminosity indicator of AGN power (Giuricin et al. 1990, Diamond-Stanic et al. 2009). On the other, H_2O line emission may be produced by amplifying the nuclear radio emission, which can provide “seed” photons for masers located on the front side of the nucleus or an associated nuclear jet (Braatz et al. 1997; Henkel et al. 1998).

In this paper, we compile radio measurements from the literature for the entire sample of reported H_2O maser host galaxies with luminosity distances $D > 0.5$ Mpc in order to investigate their radio properties and probe possible correlations between H_2O megamasers and the nuclear radio emission. The maser sample, as well as an unbiased comparison sample with no detected 22 GHz H_2O emission but good upper limits, is presented in section 2. In section 3, we analyze their radio properties. Their properties are compared, emphasizing 6 cm and 20 cm nuclear radio flux distributions and spectral indices. Furthermore, correlations

Send offprint requests to: J.S. Zhang, jszhang@gzhu.edu.cn

between maser emission and nuclear radio power are explored. These results are summarized in section 4.

2. Samples and data

2.1. The H₂O maser sample

All 85 galaxies with luminosity distances $D > 0.5$ Mpc and reported H₂O maser emission are presented in Table 2. They include 66 AGN-masers, ten SF-masers (isotropic luminosity $L_{\text{H}_2\text{O}} < 10 L_{\odot}$, known as “kilomasers”), and additional low-luminosity sources, which are still awaiting interferometric observations to identify their nature (for details of their classification and activity types, see Zhang et al. 2010). For radio continuum measurements of this maser galaxy sample, we have used the NASA Extragalactic Database (NED; <http://nedwww.ipac.caltech.edu>), the NVSS (NRAO VLA Sky Survey), and FIRST (Faint Images of the Radio Sky at Twenty-centimeters) catalogs. Since H₂O maser galaxies are mostly Seyfert 2s or LINERs, their radio continuum tends to be weak and is dominated by the circumnuclear region (Braatz et al. 1997). Most sources have been measured at 6 cm and 20 cm, while just a few sources have been observed at other wavelengths. Therefore we have collected the 6 cm and 20 cm data and use them as nuclear radio output.

The nuclear radio properties of maser host galaxies were already studied by Braatz et al. (1997). There were only 16 maser sources known at that time and just nine sources with available radio continuum data, inhibiting any detailed statistical analysis. Therefore, the current maser sample provides a drastic improvement. In Braatz et al. (1997), 6 cm VLA data measured in the A and B configurations were taken to ensure that only the small-scale flux was considered. For our current larger sample, there are no VLA observations for some sources and many sources were observed by different telescopes with different beam size. When multiple data were available, measurements were selected according to the following criteria (1) Observations with smaller beam sizes are preferred, in order to isolate the nuclear from the large scale emission of the host galaxy (Diamond-Stanic et al. 2009). This might cause missing flux when selecting interferometric data. However, the best VLA resolution at 6 cm is ~ 0.4 arcsec, which corresponds to a linear size of ~ 20 pc for a source at distance 10 Mpc. This size and the corresponding highest VLA resolution at 20 cm, ~ 2 arcsec, is much larger than that of the maser spots observed on sub-pc scales (e.g., Miyoshi et al. 1995, Reid et al. 2009) and that of potentially associated nuclear continuum sources.

(2) Both 6 cm and 20 cm data should have similar beam size. The most stringent requirement would be that data for a given source were obtained from high resolution VLA observations. Six centimeter data from the B configuration and 20 cm data from the A configuration would be optimal.

Overall, we got 6 cm data for 57 sources and 20 cm data for 79 sources. There are 55 sources with 6 cm and 20 cm data, including 41 sources with both flux densities from the same telescope. For those 41 sources, 27 have been measured with the VLA at both frequencies. Among these, 11 belong to the ideal case, with A-array 20 cm and B-array 6 cm data. For those sources with 6 cm and 20 cm data from different telescopes, the 20 cm data were taken from the VLA-D array and the 6 cm data from the Green Bank 91m (7), the Parkes 64m (6), or the MERLIN array (1). All data

with the corresponding telescopes and, if necessary, the configuration, are presented in Table 2. Below, these data are used to determine the nuclear radio fluxes and corresponding luminosities.

2.2. The nonmaser sample

As mentioned before, the detection rate of extragalactic H₂O masers is rather low (commonly $< 10\%$, e.g., Henkel et al. 2005), and it is reasonable to ask whether H₂O maser galaxies have “special” intrinsic properties, relative to apparently similar galaxies without detected maser emission. Diamond-Stanic et al. (2009) have compiled a complete sample of 89 nearby Seyfert galaxies, drawn from the unbiased revised Shapley-Ames catalog (with a limiting magnitude of $B_T < 13$ mag) (Maiolino & Rieke 1995; Ho, Filippenko & Sargent 1997). This sample is unique in that it covers mostly Seyfert 2s (like our H₂O maser sample), that it is complete, that the galaxies are rather nearby, and that sensitive H₂O measurements have been obtained toward all these targets. The distance of all those sources is less than 200 Mpc, which is comparable to that of our H₂O maser galaxies (except for the two quasar sources, SDSS J0804+3607 with $z \sim 0.66$ and MG J0414+0534 with $z \sim 2.64$, detected by Barvainis & Antonucci 2005 and Impellizzeri et al. 2008, respectively).

There are 19 maser and 70 nonmaser sources in the Seyfert comparison sample, the latter providing a useful comparison. This nonmaser sample (its sources have been targeted in H₂O maser surveys, but have not been detected) includes 16 Seyfert 1s (type 1-1.5) and 54 Seyfert 2s (type 1.8-2.0), which is similar to our maser-host Seyfert sample (most Seyfert 2s, just five Seyfert 1s (type 1-1.5), NGC 2782, UGC 5101, NGC 235A, NGC 4051 and NGC 4151). Upper limits to their maser luminosity were estimated from the RMS value (taken from the Hubble Constant Maser Experiment (HoME¹) and the Megamaser Cosmology Project (MCP²), assuming a characteristic linewidth of a spectral feature of 20 km s^{-1} and a 5σ detection threshold (e.g., Bennert et al. 2009).

The 6 cm and 20 cm radio flux densities are collected from the literature. There are 61 sources with 6 cm data and 32 sources with 20 cm data. For complementary 20 cm data, the NVSS and FIRST catalogs were also used, and we found additional 20 cm data for 17 sources and upper limits for 12 sources (with relatively low angular resolution). The nonmaser sample and corresponding data are presented in Table 3.

3. Analysis and discussion

3.1. Radio properties of H₂O maser galaxies

For our H₂O maser galaxies with available data, the distributions of nuclear radio luminosities at 6 cm and 20 cm are plotted in Figure 1. The upper panel shows the histogram of 6 cm luminosities for both the entire sample of 57 sources and the subsample of 43 AGN-masers. For the entire sample, the distribution of $\log L_{\text{6 cm}}$ peaks around 29 (here and throughout the article, $L_{\text{6 cm}}$ and $L_{\text{20 cm}}$ are

¹ <https://www.cfa.harvard.edu/~lincoln/demo/HoME>

² <https://safe.nrao.edu/wiki/bin/view/Main/MegamaserCosmologyProject> webpages

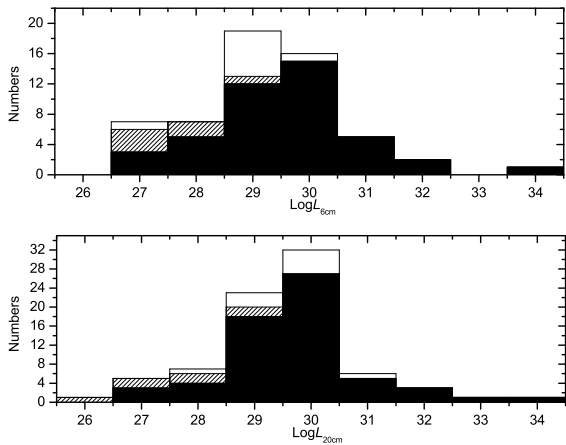


Fig. 1. The luminosity distributions of the 6 cm ($\log L_{6\text{cm}}$, upper panel) and 20 cm ($\log L_{20\text{cm}}$, lower panel) continuum emission in units of $\text{ergs}^{-1}\text{Hz}^{-1}$ for the entire maser sample, the AGN-maser subsample (shaded regions), the star formation (SF-) maser subsample (diagonal lines), and masers of unknown type.

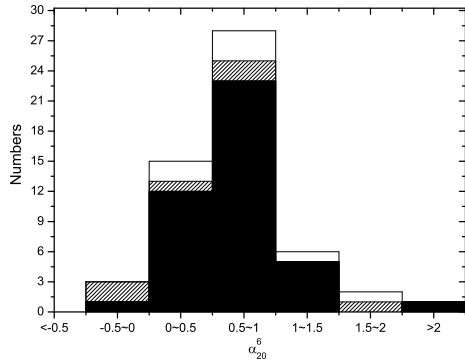


Fig. 2. Number distribution of the radio spectral index between 6 cm and 20 cm. The shaded region of the histogram represents the subsample of AGN masers. The area with diagonal lines denotes SF-masers, while the remaining masers are of unknown type.

given in units of $\text{ergs}^{-1}\text{Hz}^{-1}$) and the mean value is 28.8 ± 0.2 (Throughout the paper, given errors are the standard deviation of the mean.) The mean values are 29.0 ± 0.2 , 27.2 ± 0.4 , and 28.5 ± 0.3 for AGN-masers, SF-masers, and masers without known type, respectively. The distribution of the 20 cm luminosity is presented in the lower panel, also for all of the 79 sources and for the subsample of 56 AGN-masers, respectively. The mean value of $\log L_{20\text{cm}}$ is 29.1 ± 0.2 for the entire sample and the mean values are 29.3 ± 0.2 , 27.4 ± 0.5 , and 28.9 ± 0.2 for AGN-masers, SF-masers, and masers without known type, respectively. The subsample of AGN-disk-maser galaxies (29 sources; not shown separately, but see section 3.3) shows nuclear radio luminosities consistent with those of the entire AGN-sample. Comparing the subsamples of AGN-masers and SF-masers, a striking difference can be found between their luminosities at both 6 cm and 20 cm, i.e., AGN-masers are detected toward galaxies with higher nuclear radio luminosities.

This important point is discussed further in section 3.3.

To study the radio properties of our H₂O maser galaxies, radio spectral indices were derived for those sources for which 6 cm and 20 cm flux densities were measured. Assuming a power-law dependence for the continuum flux density given by $S \propto \nu^{-\alpha}$, the spectral index can be calculated by

$$\alpha = \log(S_{6\text{cm}}/S_{20\text{cm}}) / \log(6/20).$$

The spectral index (α) is obtained for 55 sources including 42 targets hosting AGN-masers, six objects exhibiting SF-masers, and seven sources with unknown maser type (see the second last column of Table 2). Figure 2 plots the distribution of the spectral index for those 55 maser sources and the subsamples of AGN- and SF-masers. The spectral index for the majority of sources lies in the 0.5–1.0 bin, with a mean value of 0.66 ± 0.07 . Since H₂O maser emission is mostly detected in Seyfert 2 systems, it agrees with the fact that Seyfert 2 galaxies are always steep spectrum sources. If targets with spectral index $\alpha \geq 0.3$ are defined as steep spectrum sources (Ho & Ulvestad 2001), 80% (44/55) of our maser sources belong to this category. For the subsamples of AGN-masers and SF-masers, the mean spectral indices are 0.66 ± 0.07 and 0.61 ± 0.27 , respectively. No significant difference between both distributions can be found. However, in view of the small number of SF-masers, statistical constraints are not very stringent. In addition, we note that the spectral index *might* be overestimated for those 12 sources with 6 cm data from single-dish telescopes and 20 cm data from the VLA-D array. Eliminating these sources, the mean spectral index for the remaining 32 AGN-maser sources is 0.65 ± 0.07 , while the three remaining SF sources do not justify a statistical evaluation. For the 11 sources with “optimal” data (9 AGN-masers and 2 targets of unknown type observed at 6 cm with the VLA-B and at 20 cm with the VLA A-array), the continuum appears to be flatter with a mean index value of 0.38 ± 0.12 .

3.2. Comparison of radio properties of maser and nonmaser galaxies

For the entire nonmaser sample (see Sect. 2.2; all targets are Seyfert galaxies), the mean $\log L_{6\text{cm}}$ and $\log L_{20\text{cm}}$ luminosities (in units of $\text{ergs}^{-1}\text{Hz}^{-1}$) are 27.7 ± 0.2 and 28.2 ± 0.2 , respectively. For all our maser Seyferts, the mean values are $\log L_{6\text{cm}} = 28.8 \pm 0.2$ and $\log L_{20\text{cm}} = 29.1 \pm 0.1$, respectively (see Table 1). The difference in nuclear radio luminosity between nonmaser and maser Seyferts is obvious. Considering that extragalactic H₂O masers are mostly found in Seyfert 2s, we can further compare the nuclear radio luminosities between the nonmaser Seyfert 2 subsample (36 sources) and our maser Seyfert 2 sources (41 sources). The mean values of $\log L_{6\text{cm}}$ and $\log L_{20\text{cm}}$ (again in units of $\text{ergs}^{-1}\text{Hz}^{-1}$) are 27.5 ± 0.2 and 28.0 ± 0.2 for nonmaser Seyfert 2s and 28.8 ± 0.2 and 29.1 ± 0.2 for maser Seyfert 2s, respectively. It shows the same trend, i.e., maser Seyfert 2s have higher nuclear radio luminosities than the nonmaser Seyfert 2s. The difference seems to amount to slightly more than an order of magnitude, roughly corresponding to factors of $\sim 10\text{--}20$.

To visualize the difference, we plot 6 cm versus 20 cm luminosities for both the nonmaser Seyfert sample and our

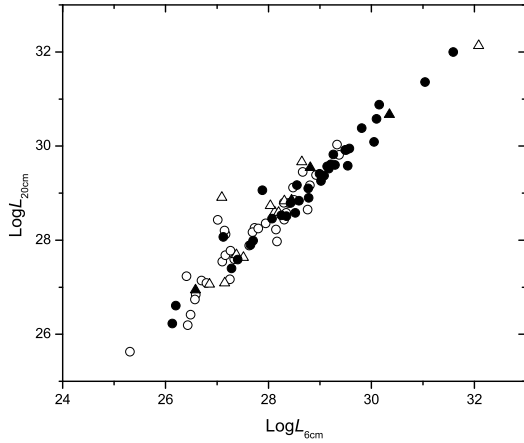


Fig. 3. Distribution of the 6 cm against the 20 cm luminosity of both the maser (filled symbols) and the nonmaser Seyfert sample (open symbols). Circles and triangles show Seyfert 2s and Seyfert 1s, respectively. Units for $L_{6\text{cm}}$ and $L_{20\text{cm}}$ are $\text{erg s}^{-1} \text{Hz}^{-1}$

maser Seyfert sample (Fig. 3). The trend is apparent. Most nonmaser sources are distributed in the lower left, while maser galaxies are mostly located in the central and upper right regions. However, there is also overlap, and there are a few maser Seyferts with low nuclear radio luminosities. This indicates that there is no strict radio continuum luminosity threshold for individual sources.

So far, we have not yet discussed a potential distance bias for the samples considered here. If measurements are very sensitive and signals strong, different distances should not play a major role with respect to detection rates. If one is, however, near the limit of sensitivity, typical luminosities of observed and classified sources should increase with the distance squared. While the average distances of the maser and nonmaser Seyfert samples show a similar range (the two distant quasars detected in H₂O by Barvainis & Antonucci 2005 and Impellizzeri et al. 2008 do not belong to any of the Seyfert samples), we find for the mean values 66.4 ± 7.5 and 31.5 ± 2.6 Mpc, respectively. Therefore, this may introduce a bias of order $(66.4/31.5)^2 \sim 4$. Even fully accounting for this effect, however, a luminosity ratio of order four still remains between the maser and the nonmaser samples.

In the nonmaser sample, there is just one source with distance >71 Mpc, while there are 20 such sources in our maser Seyfert sample. Eliminating all sources with distances >71 Mpc, the mean distances of the maser and nonmaser sample become similar (31.9 ± 3.4 Mpc versus 29.9 ± 2.1 Mpc). The mean luminosities are then $\log L_{6\text{cm}} = 28.4 \pm 0.3$ and $\log L_{20\text{cm}} = 28.7 \pm 0.2$ for our maser sample and $\log L_{6\text{cm}} = 27.7 \pm 0.2$ and $\log L_{20\text{cm}} = 27.9 \pm 0.2$ for the nonmaser sample (units: $\text{erg s}^{-1} \text{Hz}^{-1}$). The difference in their nuclear radio luminosities is still apparent (ratios of about 5 and 6 at 6 cm and 20 cm, respectively).

The luminosity ratio between the 16 H₂O detected galaxies (three additional sources show SF-related H₂O or H₂O emission of unknown type) and the 70 H₂O undetected sources in the entire Seyfert comparison sample is not affected by the Malmquist bias. Both subsamples have simi-

Table 1. A comparison of nuclear radio luminosities of maser and nonmaser galaxies (for details, see Sect. 3.2)

Samples	subsamples	$\log L_{6\text{cm}}$ ($\text{erg s}^{-1} \text{Hz}^{-1}$)	$\log L_{20\text{cm}}$ ($\text{erg s}^{-1} \text{Hz}^{-1}$)
Maser Seyferts	Total	28.8 ± 0.2	29.1 ± 0.1
	Seyfert 2	28.8 ± 0.2	29.1 ± 0.2
	$<71\text{Mpc}$	28.4 ± 0.3	28.7 ± 0.2
nonmasers (70 sources)	Total	27.7 ± 0.2	28.2 ± 0.2
	Seyfert 2	27.5 ± 0.2	28.0 ± 0.2
	$<71\text{Mpc}$	27.7 ± 0.2	27.9 ± 0.2
Non-Masers (70)	Total	27.7 ± 0.2	28.2 ± 0.2
	Seyfert 2	27.5 ± 0.2	28.0 ± 0.2
	Masers (19)	28.2 ± 0.3	28.4 ± 0.2
	Seyfert 2	28.2 ± 0.3	28.5 ± 0.2

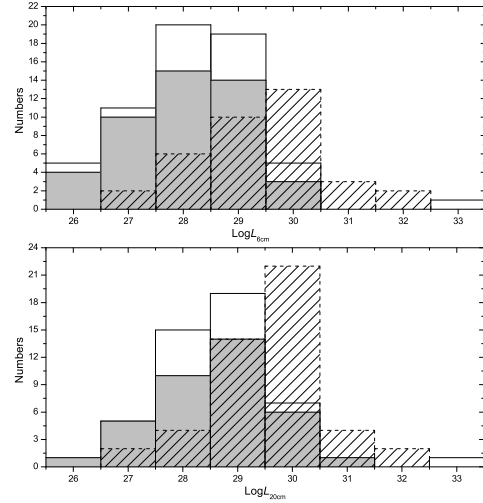


Fig. 4. Distribution of the 6 cm ($\log L_{6\text{cm}}$, upper panel) and 20 cm luminosities ($\log L_{20\text{cm}}$, lower panel) in units of $\text{erg s}^{-1} \text{Hz}^{-1}$ for the sample of nearby Seyfert galaxies without detected maser emission and its subsample of Seyfert 2s (shaded regions). For comparison, the distributions for our maser Seyfert 2s are also presented (areas filled with diagonal lines).

lar mean distances (27.5 ± 7.7 and 31.5 ± 2.6 Mpc, respectively). The mean nuclear radio luminosity of the 16 sources comprising the maser subsample ($\log L_{6\text{cm}} = 28.2 \pm 0.3$ and $\log L_{20\text{cm}} = 28.4 \pm 0.2$) is about two to three times higher than that of the 70 non-detections. The Seyfert 2 sources among these two subsamples include 15 AGN-related H₂O detections and 54 non-detections with mean distances of 28.5 ± 7.4 Mpc and 29.8 ± 2.3 Mpc, respectively. The mean luminosities on an $\text{erg s}^{-1} \text{Hz}^{-1}$ scale are $\log L_{6\text{cm}} = 28.2 \pm 0.3$ and $\log L_{20\text{cm}} = 28.5 \pm 0.3$ for the first and $\log L_{6\text{cm}} = 27.5 \pm 0.2$ and $\log L_{20\text{cm}} = 28.0 \pm 0.2$ for the second sample. The luminosity ratio is of order four (five at 6 cm and three at 20 cm). With all this evidence we thus conclude that a nuclear radio continuum luminosity ratio greater than unity is real. For a summary, see Table 1.

To visualize this result, 6 cm and 20 cm luminosity distributions are plotted for the entire nonmaser sample and its subsample comprised of Seyfert 2s in Figure 4. For comparison, the luminosity distributions for our maser Seyfert 2s are also presented. The differences are significant for the two Seyfert 2 samples and a Kolmogorov-Smirnov (KS) test shows probabilities of 0.005% at 6 cm and 0.01% at 20 cm

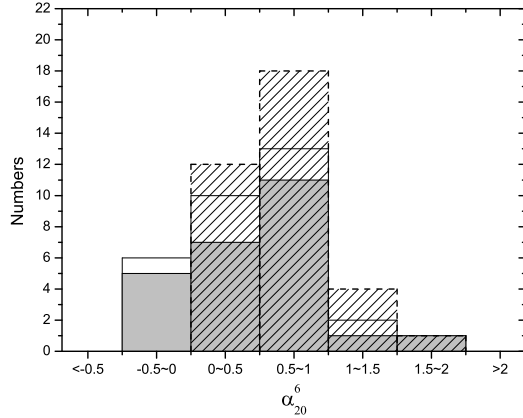


Fig. 5. The distributions of the spectral index between 6 cm and 20 cm for the nearby Seyfert sample without detected maser emission and its subsample of Seyfert 2s (shaded regions). For comparison, the distribution of Seyfert 2s with maser detections is also presented (areas filled with diagonal lines).

that both Seyfert 2 samples are drawn from the same parent population.

Similar to our maser sample, spectral indices were calculated for those 48 sources of the comparison sample (including 16 sources with 20 cm data from the NVSS or FIRST) with both 6 cm and 20 cm flux density data. The mean values of the index are 0.84 ± 0.12 and 0.83 ± 0.12 for the entire sample (48 sources) and for the Seyfert 2 subsample (36 sources). However, as mentioned before, 16 sources have low-resolution 20 cm data (from NVSS or FIRST) and high-resolution 6 cm data. This results in overestimated spectral indices for these sources, even including extremely high values (e.g., 3.47 for NGC 1097 and 2.89 for NGC 2992). After excluding those 16 sources, the mean values become 0.52 ± 0.09 for the entire sample (32 sources) and 0.55 ± 0.10 for the Seyfert 2 subsample (24 sources). Figure 5 plots the distribution of the spectral index for the nonmaser Seyfert sample (without including those 16 sources). Compared with maser host galaxies (dashed lines in Fig. 5), no significant difference can be found between the spectral index distributions. A KS test results in a probability of 79.2% that maser and nonmaser Seyfert 2 samples are drawn from the same parent distribution.

3.3. H₂O maser power v.s. nuclear radio power

Here we study possible correlations between H₂O maser line strength and AGN power. For the SF-masers alone we do not expect a correlation between the nuclear radio emission and maser power, since these maser spots are found in star-forming regions well displaced from the nuclei.

Maser luminosities, assuming here and elsewhere isotropic emission, and nuclear radio continuum fluxes are given in Table 2. In Fig. 6, these maser luminosities are plotted against 6 cm (upper panel) and 20 cm continuum luminosities (lower panel). For both panels, a correlation can be found, i.e., rising maser luminosity with increasing nuclear radio luminosity. SF-maser sources ($L_{\text{H}_2\text{O}} < 10L_{\odot}$) tend to be located in the lower left and AGN-masers (mostly

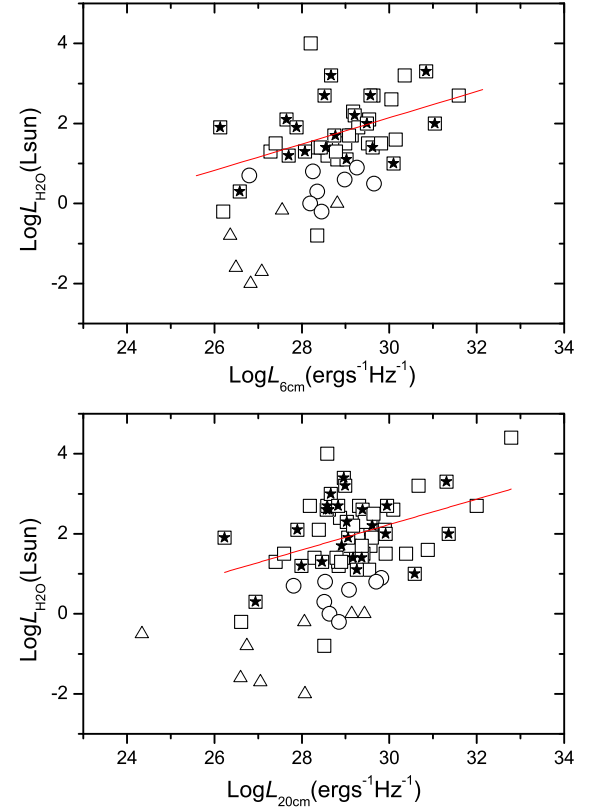


Fig. 6. H₂O maser luminosities (logarithmic scale, in L_{\odot}) against the nuclear radio luminosity (logarithmic scale, in $\text{ergs}^{-1}\text{Hz}^{-1}$) of maser host galaxies at 6 cm (upper panel) and 20 cm (lower panel). Squares, triangles, and circles represent AGN-masers, star formation-masers, and masers of unknown type, respectively. Pentacles inside squares indicate potential or confirmed disk-maser sources, which are presented in boldface in Table 2. The solid lines show linear fits to the AGN-maser sources.

$L_{\text{H}_2\text{O}} > 10L_{\odot}$) in the upper right hand corners of Fig. 6, i.e., AGN-maser galaxies tend to have higher nuclear radio luminosities relative to SF-masers (see also Sect. 3.2).

For the 6 cm continuum and 1.3 cm AGN-maser line luminosity (upper panel of Fig. 6, 41 sources), a weak correlation is apparent. A linear least-square fit shows $\log L_{\text{H}_2\text{O}} = (-7.7 \pm 3.1) + (0.3 \pm 0.1) \log L_{6\text{cm}}$, with Spearman's rank correlation coefficient $R = 0.51$ and a chance probability $P = 5.1 \times 10^{-4}$. For the 20 cm continuum and maser line luminosities (lower panel, 61 sources), our linear fitting gives $\log L_{\text{H}_2\text{O}} = (-7.3 \pm 2.7) + (0.3 \pm 0.1) \log L_{20\text{cm}}$, with the fitting parameters $R = 0.41$ and $P = 1.0 \times 10^{-3}$. As already mentioned, for many sources, the 6 cm and 20 cm data were obtained with different beam sizes (for details, see Table 2). It is thus necessary to consider this effect on the correlation. For the nine AGN-masers among those 11 sources with 'ideal' observational data (i.e., 6 cm data from the VLA-B and 20 cm data from the VLA-A configuration), the correlation becomes $\log L_{\text{H}_2\text{O}} = (-8.1 \pm 6.0) + (0.3 \pm 0.2) \log L_{6\text{cm}}$, with the fitting parameters $R = 0.51$ and $P = 0.16$. While they are too few sources for a reliable fit, the tendency to

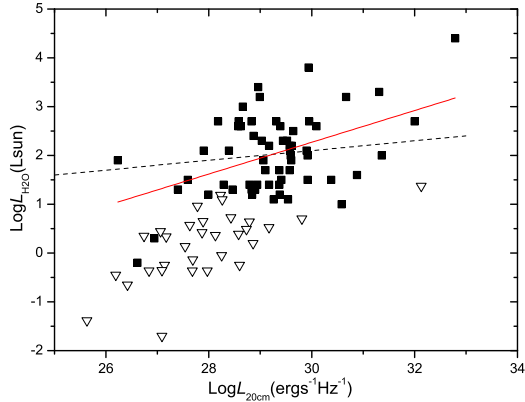


Fig. 7. H₂O maser luminosity (logarithmic scale, in L_{\odot}) versus 20 cm luminosity (logarithmic scale in $\text{ergs}^{-1}\text{Hz}^{-1}$) for AGN-masers (squares). The solid (red) and the dashed (black) lines show a linear fit without and with considering the Malmquist effect, respectively. The non-detection sample is also plotted displaying the upper limits of the maser luminosity (triangles).

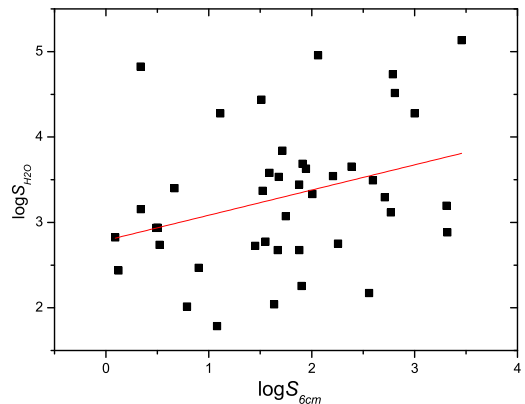


Fig. 8. Integrated H₂O flux densities (logarithmic scale, in Jy km s^{-1}) versus 6 cm luminosity (logarithmic scale in Jy) for AGN-masers (squares). The red line shows a very tentative linear fit.

ward higher continuum flux densities associated with more luminous masers is still apparent.

As a subsample of the AGN maser sources, disk maser candidates are also shown in Figure 6. These masers originate in the innermost few parsec, which might suggest a particularly close connection between their maser emission and the AGN-power. A correlation seems again to be apparent ($R=0.37$ and $P=0.13$), but the small number of disk-maser sources mean the statistical evidence is still quite weak.

We have not yet considered the Malmquist bias caused by different mean distances of galaxies comprising the samples for the luminosity-luminosity correlations. Thus we re-analyzed the relation between nuclear radio continuum and maser luminosities, using the method of partial correlation coefficients (e.g., Darling & Giovanelli 2002; Kandalyan &

Al-Zyout 2010). Since both luminosities are correlated with the variable distance, the correlations should be subtracted when we analyze the correlation between two luminosities. This type of correlation is known as a partial correlation coefficient. Figure 7 plots H₂O maser luminosity against the 20 cm nuclear radio luminosity for our AGN-maser subsample, and shows linear fits without and with considering the Malmquist effect. The correlation becomes weaker after taking the Malmquist effect into account. The correlation coefficient changes from ~ 0.3 to ~ 0.2 and the fitting becomes flatter with a slope of ~ 0.2 instead of ~ 0.3 .

For comparison, our non-detection sample with upper limits to the maser luminosity is also presented in Fig. 7. The upper limits were obtained from the individual RMS values of H₂O maser data (see details in Sect. 3.2 and Table 3). A few overlaps in maser luminosity can be found, along with H₂O undetected sources located in the lower left hand region well below the fitting line. This is consistent with the trend described in Sect. 3.2, i.e., maser activity tends to weaken with decreasing nuclear radio power.

For the AGN-maser subsample, we also correlated integrated line and continuum flux densities (for the 6 cm continuum, see Fig. 8). A linear fit yields $\log(S_{\text{H}_2\text{O}} \times \Delta V) = (0.3 \pm 0.1) \log S_{6\text{cm}} + (2.8 \pm 0.3)$ (41 sources) and $\log(S_{\text{H}_2\text{O}} \times \Delta V) = (0.2 \pm 0.1) \log S_{20\text{cm}} + (3.0 \pm 0.2)$ (56 sources), respectively, with Spearman's rank coefficients amounting to $R = 0.32$ and 0.19 and chance probabilities of $P = 0.03$ and 0.16 .

There may be a variety of causes for our statistically marginal correlations between maser and nuclear radio continuum. In the case of unsaturated H₂O maser emission only a part of the nuclear continuum may be amplified (see, e.g., the situation in NGC 4258, Herrnstein et al. 1998). For saturated maser emission, no direct correlation with the background continuum will appear. In addition, the AGN-maser sample presented here is inhomogeneous. It includes disk masers and jet masers (masers related to the interaction of nuclear radio jets with ambient molecular clouds or to the amplification of the jet's seed photons by suitably located foreground clouds), and perhaps also additional so far not yet identified maser types. The absorbing column densities along the lines of sight also differ. Among 31 AGN-masers with available data, about 60% are Compton-thick (Zhang et al. 2010). Moreover, 6 cm or 20 cm measurements as indicators of intrinsic nuclear power may introduce some uncertainties. The observed nuclear radio luminosity may depend on the geometry of the system, such as shielding by the torus. And large uncertainties may be produced from isotropically calculated H₂O maser luminosities, since maser beam angles are often poorly constrained and may be quite small due to source geometry and propagation effects (Kartje, Königl & Elitzur 1999). Lastly, uncertainties in the nuclear radio luminosity can be introduced from radio data including measurements with different resolution and sensitivity. In view of all these uncertainties, the presence of a correlation would hint at the possibility that a higher degree of activity may be able to heat up a larger volume to temperatures suitable for 22 GHz H₂O maser emission (Neufeld et al. 1994). More detailed interferometric studies are therefore required to obtain a larger sample of "ideal" data for deeper insight.

4. Summary

In this paper, the entire extragalactic 22 GHz H₂O maser sample published so far has been studied, with the notable exception of the Magellanic Clouds. Radio continuum data were analyzed to better understand the properties of the AGN associated with H₂O masers. For comparison, a complementary Seyfert sample without detected maser emission was also compiled. The main results are summarized in the following.

(1) For the entire H₂O Seyfert maser sample, the mean 6 cm and 20 cm nuclear radio luminosities are $\log L_{6\text{cm}} = 28.8 \pm 0.2$ and $\log L_{20\text{cm}} = 29.1 \pm 0.2$, respectively ($L_{6\text{cm}}, L_{20\text{cm}}$ in units of $\text{erg s}^{-1}\text{Hz}^{-1}$). For the comparison sample of Seyferts without detected maser emission, the mean values of $\log L_{6\text{cm}}$ and $\log L_{20\text{cm}}$ are 27.7 ± 0.2 and 28.2 ± 0.2 , respectively. Comparisons of corresponding subsamples also show the difference, i.e., H₂O maser sources tend to be more luminous than nonmaser sources. After considering a potential distance bias, we converged on a luminosity ratio of order five.

(2) For the H₂O maser sample and the sample of Seyferts devoid of detected H₂O emission, spectral indices were derived from the 6 cm and 20 cm data. There is no significant difference for the distributions of the spectral indices between our H₂O maser sources and the H₂O undetected sources. The mean value of the index is 0.66 ± 0.07 for our H₂O maser sample and 0.52 ± 0.09 for the comparison sample.

(3) For the subsample of AGN-masers, a correlation seems to be present between H₂O maser isotropic luminosity and nuclear radio power of the host galaxy. However, the correlation is significantly affected by the Malmquist bias so that no definite conclusion can be drawn right now.

(4) Based on the results outlined above, the nuclear radio luminosity may provide a clear signature of AGN-masers, possibly providing suitable constraints for future H₂O megamaser surveys.

Acknowledgements. This work is supported by the Natural Science Foundation of China (No. 11043012, 11178009) and China Ministry of Science and Technology under State Key Development Program for Basic Research (2012CB821800). We made use of the NASA Astrophysics Data System Bibliographic Services (ADS) and the NASA/IPAC extragalactic Database (NED), which is operated by the Jet Propulsion Laboratory, California Institute of Technology, under contract with NASA.

References

Baan, W. A. & Klöckner, H. R. 2006, A&A 449, 559

Barvainis, R., & Antonucci, R. 2005, ApJ, 628, L89

Becker, R.H., White, R.L. & Edwards, A.L. 1991, ApJS, 75, 229

Becker, R.H., White, R.L. & Helfand, D.J. 1995, ApJ, 450, 559

Bennert, N., Barvanis, R., Henkel, C. & Antonucci, R. 2009, ApJ, 695, 276

Bordalo, V., Plana, H. & Telles, E. 2009, ApJ, 696, 1668

Braatz, J.A., Condon, J.J., Henkel, C., Lo, K.-Y. & Reid, M.J. 2009, Astro2010, 23

Braatz, J.A. & Gugliucci, N.E. 2008, ApJ, 678, 96

Braatz, J.A., Wilson, A.S. & Henkel, C. 1997, ApJS, 110, 321

Bransford, M.A., Appleton, P.N., Heisler, C.A., Norris, R.P. & Marston, A.P. 1998, ApJ, 497, 133

Churchwell, E., Witzel, A., Huchtmeier, W., Pauliny-Toth, I., Roland, J. & Sieber, W. 1977, A&A 54, 969

Condon, J.J. 1983, ApJS, 53, 459

Condon, J.J., Cotton, W.D. & Broderick, J.J. 2002, AJ, 124, 675

Condon, J.J., Cotton, W.D., Greisen, E.W., Yin, Q.F., Perley, R.A., Taylor, G.B. & Broderick, J.J. 1998, AJ, 115, 1693

Condon, J.J., Helou, G., Sanders, D.B. & Soifer, B.T. 1996, ApJS, 103, 81

Cooper, N.J., Lister, M.L. & Kochanczyk, M.D. 2007, ApJS, 171, 376

Darling, J., Brogan, C. & Johnson, K. 2008, ApJS, 685, 39

Diamond-Stanic, A.M., Rieke, G.H. & Rigby, J.R. 2009, ApJ, 698, 623

Filho, M.E., Barthel, P.D. & Ho, L.C. 2006, A&A 451, 71

Gallimore, J.F., Axon, D.J., O'Dea, C.P., Baum, S.A. & Pedlar, A. 2006, AJ, 132, 546

Giuricin, G., Mardirossian, F., Mezzetti, M. & Bertotti, G. 1990, ApJS, 72, 551

Greenhill, L.J., Tilak, A. & Madejski, G. 2008, ApJ, 686, L13

Gregory, P.C. & Condon, J.J. 1991, ApJS, 75, 1011

Griffith, M.R., Wright, A.E., Burke, B.F. & Ekers, R.D. 1995, ApJS, 97, 347

Guo, Q., Zhang, J.S. & Fan, J.H. 2009, IJMPD, 1809, 1367

Haschick, A.D., Baan, W.A., Schneps, M.H. et al., ApJ, 356, 149

Henkel, C., Wang, Y.-P., Falcke, H., Wilson, A.S. & Braatz, J.A. 1998, A&A, 335, 463

Henkel, C., Peck, A.B., Tarchi, A., Nagar, N. M., Braatz, J.A., Castangia, P. & Moscadelli, L. 2005, A&A, 436, 75

Herrnstein, J.R., Greenhill, L.J., Moran, J.M. et al. 1998, ApJ, 497, L69

Ho, L.C., Filippenko, A.V. & Sargent, W.L.W. 1997, ApJS, 112, 31

Ho, L.C. & Ulvestad, J.S. 2001, ApJS, 133, 77

Impellizzeri, C.M.V., McKean, J.P., Castangia, P., Roy, A.L., Henkel, C., Brunthaler, A. & Wucknitz, O. 2008, Nature, 456, 927

Kandalyan, R.A. & M. Al-Zyout 2010, Astrophysics, 53, 475

Kartje, J.F., Königl, A. & Elitzur M. 1999, ApJ, 513, 180

Kobulnicky, H.A. & Johnson, K.E. 1999, ApJ, 527, 154

Kondratko, P.T., Greenhill, L.J. & Moran, J.M. 2006, ApJ, 638, 100

Lo, K.Y. 2005, ARA&A, 43, 625

Maiolino, R. & Rieke, G.H. 1995, ApJ, 454, 95

Miyoshi, M., Moran, J., Herrnstein, J., et al. 1995, Nature, 373, 127

Morganti, R., Tsvetanov, Z.I., Gallimore, J. & Allen, M.G. 1999, A&AS, 137, 457

Neff, S.G. & Hutchings, J.B. 1992, ApJ, 103, 1746

Neff, S.G., Ulvestad, J.S. & Teng, S.H. 2004, ApJ, 611, 186

Neufeld, D. A., Maloney, P. R. & Conger, S. 1994, ApJ, 436, L127

Oosterloo, T.A., Morganti, R., Sadler, E.M., van der Hulst, T. & Serra, P. 2007, A&A 465, 787

Reid, M.J., Braatz, J.A., Condon, J.J., Greenhill, L.J., Henkel, C. & Lo, K.Y. 2009, ApJ, 695, 287

Sadler, E.M., Slee, O.B., Reynolds, J.E. & Roy, A.L. 1995, MNRAS, 276, 1373

Sandqvist, A., Joersaeter, S. & Lindblad, P.O. 1995, A&A 295, 58

Schmitt, H.R., Ulvestad, J.S., Antonucci, R.R.J. & Kinney, A.L. 2001, ApJS, 132, 199

Slee, O.B., Sadler, E.M., Reynolds, J.E. & Ekers, R.D. 1994, MNRAS, 269, 928

Tarchi, A., Castangia, P., Henkel, C., Surcis, G. & Menten, K.M. 2011, 525, 91

Taylor, G.B., Peck, A.B., Henkel, C., Falcke, H., Mundell, C.G., O'Dea, C.P., Baum, S.A. & Gallimore, J.F. 2002, ApJ, 574, 88

Thean, A., Pedlar, A., Kukula, M.J., Kukula, M.J., Baum, S.A., O'Dea & Christopher P. 2000, MNRAS, 314, 573

Ulvestad, J.S. & Wilson, A.S. 1984a, ApJ, 278, 544

Ulvestad, J.S. & Wilson, A.S. 1984b, ApJ, 285, 439

Ulvestad, J.S. & Wilson, A.S. 1989, ApJ, 343, 659

Vila, M.B., Pedlar, A. & Davies, R.D. 1990, MNRAS, 242, 379

White, R.L. & Becker, R.H. 1992, ApJS, 79, 331

Wilson, A.S., Pooley, G.G., Clements, E.D. & Willis, A.G. 1980, ApJ, 237, 61

Wright, A. & Otrupcek, R. 1990, PKSCAT90

Wright, A.E., Griffith, M.R., Burke, B.F. & Ekers, R.D. 1994, ApJS, 91, 111

Wright, A.E., Griffith, M.R., Hunt, A.J., Troup, E., Burke, B.F. & Ekers, R.D. 1996, ApJS, 103, 145

Zhang, J.S., Henkel, C., Guo, Q., Wang, H.G. & Fan, J.H. 2010, ApJ, 708, 1528

Zhang, J.S., Henkel, C., Kadler, M., Greenhill, L.J., Nagar, N., Wilson, A.S. & Braatz, J.A. 2006, A&A, 450, 933

Zijlstra, A., Pottasch, S. & Bignell, C. 1990, A&AS, 82, 273

Table 2. Radio properties of H₂O maser host galaxies*

Source	Type	D	S ₆	Tel./Ref.	S ₂₀	Tel./Ref.	α	log L _{H₂O}
NGC 17	Sy2	79.1			67.5 \pm 2.5	VLA-D/Con98	0.8	
NGC 23	LINER	60.9	33.0 \pm 5	GB/Bec91	74.3 \pm 2.7	VLA-D/Con98	0.67	2.3
<i>IC 10</i>		1.2	137.0 \pm 14	GB/Gre91	319.0	GB/Whi92	0.70	-0.8
NGC 0235A	Sy1	86.90			42.6 \pm 1.4	VLA-D/Con98	2.0	
NGC 253	Sy2,SBG	3	2080.0	Parkes/Wri90	2994.7 \pm 113.5	VLA-D/Con98	0.30	-0.8
NGC 262 (Mrk 348)	Sy2	62.00	244.0 \pm 3.7	GB/Gre91	292.7 \pm 8.8	VLA-D/Con98	0.08	2.6
IRAS F01063-8034		67	81.0 \pm 7	Parkes/Wri94				2.7
NGC 449 (Mrk 1)	Sy2	64	28.0 \pm 2	VLA-A/Ulv84a	75.9 \pm 2.3	VLA-D/Con98	0.83	1.7
NGC 520	SBG	27	90.0 \pm 14	GB/Bec91	182.0	VLA-D/Con98	0.28	0.3
<i>NGC 598(M 33)</i>	H II	0.7			3.7 \pm 0.6	VLA-D/Con98		-0.5
NGC 591	Sy2	61	7.9	VLA-A/Ulv89	24.5	VLA-A/Ulv89	0.9	1.4
NGC 0613	Sy2	17.9	101.0 \pm 13	Parkes/Wri96	179.6	VLA-D/Con98	0.48	1.2
<i>IC 0184</i>	Sy2	70.5			3.3 \pm 0.5	VLA-D/Con98		1.4
NGC 1052	Sy2,LINER	17	1000.0	VLA-A/Bra97	1103.0	VLA-A/Coo07	0.08	2.1
NGC 1068	Sy2,Sy1	14.5	644.0	VLA-B/Ho01	1630.0	VLA-A/Ho01	0.77	2.2
NGC 1106	Sy2	57.8	46.0 \pm 6.9	GB/Gre91	166.0	GB/Whi92	1.07	0.9
Mrk 1066	Sy2	48	35.5	VLA-A/Ulv89	94.3	VLA-A/Ulv89	0.81	1.5
NGC 1320	Sy2	35.5	3.3	VLA-D/Gal06	6.5 \pm 0.6	VLA-D/Con98	0.56	1.2
NGC 1386	Sy2	17	13.0	VLA-A/Ulv84b	23.0	VLA-A/Ulv84b	0.47	2.1
IRAS 03355+0104	Sy2	159.1			26.5 \pm 1.3	VLA-D/Con98		2.1
<i>IC 342</i>	Sy2	2	277.0 \pm 41.5	GB/Gre91	2475.0	GB/Whi92	1.82	-2.0
MG J0414+0534	QSO1	10836	1119.0 \pm 167	GB/Bec91	2676.0	GB/Whi92	0.72	4.0
UGC 3193		59.4			17.7 \pm 0.7	VLA-D/Con98		2.4
UGC 3255	Sy2	75			35.8 \pm 1.2	VLA-D/Con98		1.2
Mrk 3	Sy2	54	361.0 \pm 30	VLA-A/Wil80	1100.9 \pm 33	VLA-D/Con98	0.93	1.0
<i>NGC 2146</i>	H II	14.5			1074.5 \pm 40	VLA-D/Con98		0.0
VII ZW 073	Sy2	158.9			12.4 \pm 0.6	VLA-D/Con98		2.2
NGC 2273	Sy2	24.5	24.5	VLA-B/Ho01	47.3	VLA-A/Ho01	0.55	0.8
UGC 3789	Sy2	44.3			17.6 \pm 1.0	VLA-D/Con98		2.6
Mrk 78	Sy2	150	12.0 \pm 2	VLA-A/Ulv84a	31.0 \pm 3	VLA-A/Ulv84a	0.79	1.5
J0804+3607	QSO2	2640			73.7	VLA-B/Bec95		4.4
<i>He 2-10</i>	SBG	10.5	27.0 \pm 0.11	VLA-B/Zij90	21.1 \pm 1.2	VLA-BnA/Kob99	-0.2	-0.2
2MASX J08362280	Sy2	197.4			2.0	VLA-B/Bec95		3.4
Mrk 1210	Sy2,Sy1	54	56.0 \pm 10	GB/Bec91	114.0	VLA-D/Con02	0.59	1.9
NGC 2639	LINER	44	182.0	VLA-B/Ho01	102	VLA-A/Ho01	-0.48	1.4
NGC 2782	Sy1,SBG	34	47.0 \pm 7.0	GB/Bec91	252.0	GB/Whi92	1.39	1.1
NGC 2824 (Mrk 394)	Sy?	37			9.3 \pm 0.5	VLA-D/Con98		2.7
SBS 0927+493	LINER	135.6			9.3 \pm 0.5	VLA-D/Con98		2.7
NGC 2960	LINER	66			7.1	VLA-D/Con02		2.6
UGC 5101	LINER,Sy1.5	157.4	76.0 \pm 11.4	GB/Bec91	158.0	GB/Whi92	0.61	3.2
NGC 2979	Sy2	36			15.7 \pm 1.0	VLA-D/Con02		2.1
NGC 2989	H II	55.3			18.6 \pm 1.5	VLA-D/Con02		1.6
<i>NGC 3034(M 82)</i>	SBG	3.7	3957.0 \pm 59	GB/Bec91	8363.0	GB/Whi92	0.62	0.0
NGC 3079	Sy2,LINER	15.5	114.0	VLA-B/Ho01	132.0	VLA-A/Ho01	0.12	2.7
Mrk 34	Sy2	205	6.1	VLA-A/Ulv84a	16.5	VLA-A/Ulv84a	0.83	2.0
<i>NGC 3359</i>	H II	13.5			52.9	VLA-D/Con02		-0.2
IC 2560	Sy2	35			31.0	NVSS		3.0
NGC 3393	Sy2	50	52 \pm 11	Parkes/Gri94	81.5 \pm 3.3	VLA-D/Con98	0.37	2.6
NGC 3556	H II	12	90.0 \pm 13	GB/Gre91	245.0	GB/Whi92	0.83	0.0
Arp 299 (NGC 3690)	SBG	42	11.1 \pm 0.6	VLA-A/Neff04	41.6 \pm 2.1	VLA-A/Neff04	1.1	1.4
NGC 3735	Sy2	36	1.24	VLA-B/Ho01	1.61	VLA-A/Ho01	0.22	1.3
<i>Antennae</i>	SBG	20						0.9
NGC 4051	Sy1.5	10	3.2	VLA-B/Ho01	7.4	VLA-A/Ho01	0.69	0.3
NGC 4151	Sy1.5	13.5	129.0	VLA-B/Ho01	324.0	VLA-A/Ho01	0.76	-0.2
<i>NGC 4214</i>	SBG	2.94	30.0 \pm 7	GB/Bec91	38.3	VLA-D/Con02	0.2	-1.6
NGC 4258	Sy1.9,LINER	7.2	2.2	VLA-B/Ho01	2.7	VLA-A/Ho01	0.19	1.9
NGC 4293	LINER	17	1.8	MERLIN/Fil06	18.5	VLA-D/Con02	1.93	0.7
NGC 4388	Sy2	34	26.9	VLA-B/Ho01	43.3	VLA-A/Ho01	0.40	1.1
NGC 4527	LINER	23.1	151 \pm 22.5	GB/Gre91	187.9	VLA-D/Con02	0.18	0.6
ESO 269-G012	Sy2	66			<3.7	ATCA/Oos07		3.0
NGC 4922	Sy2,LINER	95			40.1	FIRST		2.3
NGC 4945	Sy2	4	2840	Parkes/Wri90	6600	Parkes/Wri90	0.26	1.7
NGC 5194 (M 51)	Sy2	10	1.3	VLA-B/Ho01	3.4	VLA-A/Ho01	0.8	-0.2
NGC 5253	SBG	3.33	90 \pm 12	Parkes/Wri96	83.8	VLA-D/Con96	-0.06	-1.7
NGC 5256 (Mrk 266)	Sy2,SBG	112	43.3 \pm 2.2	GB/Bec91	159.0	GB/Gre91	1.08	1.5
NGC 5347	Sy2	31	2.2	VLA-A/Ulv89	3.4	VLA-A/Ulv89	0.36	1.5
NGC 5495	Sy2	87.9			11.5	NVSS		2.3
Circinus	Sy2	4	610.0	Parkes/Wri90	1500.0	Parkes/Wri90	0.75	1.3
NGC 5506 (Mrk1376)	Sy1.9	25	160.0 \pm 8.0	VLA-A/Ulv84b	315.0	VLA-A/Ulv84b	0.56	1.7
NGC 5643	Sy2	16	87.0 \pm 10	Parkes/Wri94	203.0	VLA-D/Con96	0.7	1.4
NGC 5728	Sy2	37	4.6	VLA-A/Ulv89	70.0	NVSS	2.26	1.9
UGC09618NED02	LINER	134.6	39.0 \pm 6.0	GB/Bec91	81.6	VLA-D/Con02	0.61	3.2
NGC 5793	Sy2	47	508.0	VLA-A/Ban06	1047.0	VLA-A/Ban06	0.6	2.0
NGC 6240	Sy2	98	80.0	VLA-A/Bra97	426.0	VLA-D/Con02	1.39	1.6
NGC 6264	Sy2	135.7			<0.9	FIRST		3.1
NGC 6300	Sy2	15	39.0 \pm 7.0	Parkes/Wri94				0.5
NGC 6323	Sy2	104			3.1	VLA-D/Con02		2.7
ESO 103-G035	Sy2	53						2.6
IRAS F19370-0131	Sy2	80						
3C 403	FR II	235	2026.0 \pm 283	GB/Gre91	5798.0	GB/Whi92	0.9	3.3
NGC 6926	Sy2	80	48.0 \pm 11	Parkes/Gri95	117.0	VLA-D/Con02	0.74	2.7
AM2158-380NED02	Sy2	128.8	590.0	Parkes/Wri90	1530.0	Parkes/Wri90	0.79	2.7
TXS 2226-184	LINER	100	32.2 \pm 0.98	VLA-B/Tay02	73.3 \pm 2.2	VLA-B/Tay02	0.68	3.8
NGC 7479	Sy2	31.8	3.1	VLA-B/Ho01	4.0	VLA-A/Ho01	0.21	1.3

Table 2. continued.

Source	Type	D	S ₆	Tel./Ref.	S ₂₀	Tel./Ref.	α	log L _{H₂O}
IC 1481	LINER	82			36.2	VLA-D/Con02		2.5

* Radio properties for the published extragalactic H₂O maser host galaxies with luminosity distance $D > 0.5$ Mpc (Zhang et al. 2010). Ten masers associated with star-forming regions are presented in italics and 29 disk-maser candidates in boldface.

Column 1: Source; For Arp 299, the emission from NGC 3690 was only taken (Neff et al. 2004; Tarchi et al. 2011).

Column 2: Types of nuclear activity from Zhang et al. (2010). SBG: starburst galaxy; Sy1.5, Sy1.9, Sy2: Seyfert type; LINER: low-ionization nuclear emission line region; ULIRG: ultra luminous infrared galaxy; FR II: Fanaroff-Riley type II radio galaxy; H II: H II galaxies, i.e., dwarf galaxies undergoing a burst of star formation (i.e., Bordalo et al. 2009);

Column 3: The luminosity distance in Mpc, assuming $H_0 = 75 \text{ km s}^{-1} \text{ Mpc}^{-1}$. For the high z objects (SDSS J0804+3607 and J0414+0534), $\Omega_M = 0.270$ and $\Omega_{vac} = 0.730$. 78 sources from Bennert et al. (2009), MG J0414+0534 from Impellizzeri et al. (2008), NGC 17 and NGC 1320 from Greenhill et al. (2008), He 2-10, the Antennae, NGC 4214 and NGC 5253 from Darling et al. (2008);

Columns 4 and 6: The 6 cm and 20 cm radio flux densities with uncertainties (if available) in mJy from “Photometry & SEDs” in NED;

Columns 5 and 7: Tel./Ref., used telescopes and corresponding reference for the 6 cm and 20 cm flux density. GB: Green Bank 91m telescope; VLA-A, -B, -C, -D: Very Large Array and used configuration; Parkes: the Parkes 64-m radio telescope; MERLIN: the multi-element radio-linked interferometer network; ATCA: Australian telescope compact array; NVSS: NRAO VLA sky survey catalog; FIRST: faint images of the radio sky at twenty-centimeters catalog; Ban06: Bann & Klöckner (2006); Bec91: Becker et al. (1991); Bec95: Becker et al. (1995); Bra97: Braatz et al. (1997); Con83: Condon (1983); Con96: Condon et al. (1996); Con98: Condon et al. (1998); Con02: Condon et al. (2002); Coo07: Cooper et al. (2007); Fil06: Filho et al. (2006); Gal06: Gallimore et al. (2006); Gre91: Gregory & Condon (1991); Gri95: Griffith et al. (1995); Ho01: Ho & Ulvestad (2001); Kob99: Kobulnicky & Johnson 1999; Neff04: Neff et al. (2004); Oos07: Oosterloo et al. (2007); Tay02: Taylor et al. (2002); Ulv84a: Ulvestad & Wilson (1984a); Ulv84b: Ulvestad & Wilson (1984b); Ulv89: Ulvestad & Wilson (1989); Whi92: White & Becker (1992); Wil80: Wilson et al. (1980); Wri90: Wright & Otrupcek (1990); Wri94: Wright et al. (1994); Wri96: Wright et al. (1996); Zij90: Zijlstra et al. (1990);

Column 8: The spectral index between 6 cm and 20 cm, assuming $S \propto \nu^{-\alpha}$;

Column 9: The apparent luminosity of maser emission (on a logarithmic scale), in units of L_\odot , taken from Bennert et al. (2009), Darling et al. (2008), Greenhill et al. (2008), and Tarchi et al. (2011).

Table 3. Radio properties of Seyfert galaxies without detected H₂O maser*

Source	Type	D	S ₆	S ₂₀	Reference	α	RMS-H ₂ O	UL-H ₂ O
NGC 777	2	66.5	2.63	3.19	Ho01	0.16	6.9	1.2
NGC 788	2	54.1	1.2	2.2	Ulv89	0.50	3	0.6
NGC 1058	2	9.2	<0.12	6.9	Ho01, NVSS		20.0	-0.1
NGC 1097	1.0	16.5	3.8	249.2	Mor99, NVSS	3.47	15	0.3
NGC 1241	2	53.8	6.8		The00		7.4	1.0
NGC 1275	1.5	70.1	20700	23200	Ho01	0.09	9.5	1.4
NGC 1365	1.8	21.5	0.9	2.5	San95	0.85	2.4	-0.2
NGC 1358	2	53.6	7.04	17.9	Ho01	0.78	3	0.6
NGC 1433	2	13.3	<3.0		Sad95		15	0.1
NGC 1566	1.5	19.4	<6.0		Sad95		12	0.4
NGC 1667	2	61.2	1.19	4.08	Ho01	1.02	6.6	1.1
NGC 2685	2	16.2	<0.13	<1.0	Ho01, FIRST		19.0	0.4
NGC 2655	2	24.4	44.1	101	Ho01	0.69	5.2	0.2
NGC 2992	1.9	34.1	7.0	226.2	Sad95, NVSS	2.89	2.3	0.1
NGC 3031	1.5	3.6	91.2	79.2	Ho01	-0.12	3.0	-1.7
NGC 3081	2	34.2	0.9	2.5	Ulv89	0.85	2.3	0.1
NGC 3147	2	40.9	10.1	13.6	Ho01	0.25	6.3	0.7
NGC 3185	2	21.3	0.47	3.16	Ho01, FIRST	1.58	3	-0.2
NGC 3227	1.5	20.6	25.9	78.2	Ho01	0.92	2.6	-0.2
NGC 3254	2	23.6	<0.12	<0.84	Ho01, FIRST		28	0.9
NGC 3281	2	44.7	26.7	61.2	Ulv89	0.69	3.3	0.5
NGC 3486	2	7.4	<0.12	<0.95	Ho01, FIRST		21	-0.2
NGC 3516	1.2	38.9	6.03	29.8	Ho01	1.33	4	0.5
IRAS11215	2	62.4	18	52.1	Sch01, NVSS	0.88	20	1.6
NGC 3783	1.2	36.1	13	43.6	Sad95, NVSS	1.01	5	0.5
NGC 3941	2	18.9	0.19	<0.97	Ho01, FIRST		22	0.6
NGC 3976	2	37.7	0.41	<0.95	Ho01, FIRST		16	1.1
NGC 3982	1.9	17.0	1.79	3.56	Ho01	0.57	3.0	-0.4
NGC 4138	1.9	17.0	0.78	0.45	Ho01	-0.46	2.4	-0.5
NGC 4168	1.9	16.8	5.24	4.37	Ho01	-0.15	15.0	0.3
NGC 4235	1.2	35.1	5.61	5.05	Ho01	-0.09	4.2	0.4
NGC 4378	2	35.1	0.21	<0.94	Ho01, FIRST		15.0	1.0
NGC 4395	1.8	4.6	0.80	1.68	Ho01	0.62	3.8	-1.4
NGC 4472	2	16.8	65.2	113	Ho01	0.46	17.0	0.4
NGC 4477	2	16.8	0.18	<0.97	Ho01, FIRST		4.2	-0.2
NGC 4501	2	16.8	1.14	2.06	Ho01	0.49	3.0	-0.4
NGC 4507	2	59.6	10.8	66.1	Bra98, NVSS	1.50	9.8	1.2
NGC 4565	1.9	9.7	2.72	2.31	Ho01	-0.14	4.6	-0.7
NGC 4579	1.9	16.8	43.1	27.8	Ho01	-0.36	3.0	-0.4
NGC 4593	1.0	41.3	1.6	2.1	Ulv84b	0.23	4.3	0.6
NGC 4594	1.9	20.0	120	93.4	Sad95, NVSS	-0.21	13.0	0.4
IC 3639	2	35.3	20	87.9	Sad95, NVSS	1.23	18.0	1.1
NGC 4639	1.0	16.8	0.15	<0.84	Ho01, FIRST		16	0.4
NGC 4698	2	16.8	0.23	<1.01	Ho01, FIRST		16	0.4
NGC 4725	2	12.4	<0.17	<0.97	Ho01, FIRST		4.1	-0.5
NGC 4941	2	16.8	4.3	14.2	Ulv89	0.99	3	-0.4
NGC 4939	2	46.6	0.7	2.3	Vil90	0.99	8.3	1.0
NGC 5005	2	21.3	2.7	24.6	Vil90	1.84	10	0.4
NGC 5033	1.5	18.7	5.68	11.7	Ho01	0.60	4.1	-0.1
NGC 5128	2	4.3	6456		Sle94		3	-1.5
NGC 5135	2	57.7	58.8	163.2	Ulv89	0.85	3	0.7
NGC 5273	1.5	21.3	1.31	2.13	Ho01	0.40	12	0.4
NGC 5395	2	46.7	0.19	<0.92	Ho01, FIRST		4.1	0.7
NGC 5427	2	40.4	2.5	7.54	Mor99, FIRST	0.92	3	0.4
NGC 5631	2	32.7	0.29	0.43	Ho01	0.33	4.1	0.3
NGC 5899	2	42.8	4.0	10.35	Dia09, FIRST	0.79	3	0.4
NGC 6221	2	19.3	<1.0		Sad95		11	0.3
NGC 6814	1.5	25.6	20	49.7	Sad95, NVSS	0.76	5.8	0.3
NGC 6951	2	24.1	9.05	25.5	Ho01	0.86	3	-0.1
MRK 509	1.2	143.8	1.8	18.6	Nef92, NVSS	1.94	2.7	1.4
NGC 7130	2	68.7	38	189.7	Sad95, NVSS	1.34	16	1.6
NGC 7172	2	37.6	11.7	36.8	Mor99, NVSS	0.95	6.7	0.7
NGC 7213	1.5	24.9	207		Bra98		14	0.6
NGC 7314	1.9	20.8	2.7	31.0	Mor99, NVSS	2.03	7.4	0.2
NGC 7410	2	24.8	1.4	36.8	Con98, NVSS	2.72	14	0.6
NGC 7469	1.2	67.0	21	<0.88	Sad95, FIRST		2.9	0.8
NGC 7496	2	23.1	3.8		The00		15	0.6
NGC 7582	2	22.0	69		Sad95		10.9	0.4
NGC 7590	2	22.0	<0.3		The00		15	0.6
NGC 7743	2	24.4	3.03	5.52	Ho01	0.50	3	0.0

* Radio properties for the nearby nonmaser Seyfert galaxy sample, including 16 Seyfert 1s (type 1-1.5) and 54 Seyfert 2s (type 1.8-2.0).

Column 1: Source;

Column 2: Seyfert type, optical classification from Maiolino & Rieke (1995) or Ho et al. (1997);

Column 3: Distance in Mpc, taken from Diamond-Stanic et al. (2009);

Column 4: 6 cm radio flux density in mJy;

Column 5: 20 cm radio flux density in mJy;

Column 6: References for Cols. 4&5 (For sources without available 20 cm data in the literature, their 20 cm data are taken from the NVSS or FIRST catalog.): Ho01: Ho & Ulvestad (2001); Ulv89: Ulvestad & Wilson (1989); Mor99: Morganti et al. (1999); The00: Thean et al. (2000); Sad95: Sadler et al. (1995); San95: Sandqvist et al. (1995); Sch01: Schmitt et al. (2001); Bra98: Bransford et al. (1998); Ulv84b: Ulvestad & Wilson (1984b); Vil90: Vila et al. (1990); Sle94: Slez et al. (1984); Dia09: Diamond-Stanic et al. (2009); Nef92: Neff & Hutchings (1992); Con98: Condon et al. (1998);

Column 7: the spectral index between 6 cm and 20 cm, derived from the values in Cols. 4&5, assuming $S \propto \nu^{-\alpha}$;

Column 8: RMS values of H₂O maser data in units of *mJy*, which were taken from MCP and HoME webpages. GBT observations are taken whenever possible and in case of several observations the GBT spectrum with the lowest RMS value was selected;

Column 9: Estimated upper limits of H₂O maser luminosity ($\log L_{\text{H}_2\text{O}}$, in units of L_{\odot}) for nonmaser Seyfert galaxies, from the RMS value (Column 8), see details in Section 3.2.